A light-stimulated synaptic device based on graphene hybrid phototransistor

2017 2D Mater. 4 035022

(http://iopscience.iop.org/2053-1583/4/3/035022)

2D Materials

PAPER

RECEIVED
23 May 2017

REVISED
5 July 2017

ACCEPTED FOR PUBLICATION
18 July 2017

PUBLISHED
2 August 2017

A light-stimulated synaptic device based on graphene hybrid phototransistor

Shuchao Qin[1], Fengqiu Wang[1], Yujie Liu, Qing Wan, Xinran Wang, Yongbing Xu, Yi Shi, Xiaomu Wang and Rong Zhang

School of Electronic Science and Engineering and Collaborative Innovation Center of Advanced Microstructures, Nanjing University, Nanjing 210093, People's Republic of China

[1] These authors contributed equally to this work.

E-mail: fwang@nju.edu.cn, xiaomu.wang@nju.edu.cn and rzhang@nju.edu.cn

Keywords: 2d heterostructure, artificial synapse, neural network, optical signal processing, graphene-carbon nanotube hybrid

Supplementary material for this article is available online

Abstract

Neuromorphic chips refer to an unconventional computing architecture that is modelled on biological brains. They are increasingly employed for processing sensory data for machine vision, context cognition, and decision making. Despite rapid advances, neuromorphic computing has remained largely an electronic technology, making it a challenge to access the superior computing features provided by photons, or to directly process vision data that has increasing importance to artificial intelligence. Here we report a novel light-stimulated synaptic device based on a graphene-carbon nanotube hybrid phototransistor. Significantly, the device can respond to optical stimuli in a highly neuron-like fashion and exhibits flexible tuning of both short- and long-term plasticity. These features combined with the spatiotemporal processability make our device a capable counterpart to today's electrically-driven artificial synapses, with superior reconfigurable capabilities. In addition, our device allows for generic optical spike processing, which provides a foundation for more sophisticated computing. The silicon-compatible, multifunctional photosensitive synapse opens up a new opportunity for neural networks enabled by photonics and extends current neuromorphic systems in terms of system complexities and functionalities.

1. Introduction

Inspired by biological neural systems, neuromorphic chips [1–3] are rapidly developed as a viable technological avenue in artificial intelligence. In contrast to traditional von Neumann computers, neuromorphic devices are well suited to interact with sensory data in humanlike ways [1, 4]. This renders neuromorphic chips extremely effective for solving complex tasks such as image recognition, multi-object detection and visual signal classification. In biological neural systems, synapses are the most fundamental computing element. Notably, the connectivity or response of synapses depends on stimuli previously experienced [5]. The changing of the connectivity, known as synaptic plasticity, is responsible for both short- and long-term memory behaviors, and a large number of synapses collectively produce functionally significant operations [6]. Inspired by such biological systems, several artificial synaptic devices have been developed based on either transistors [4, 7–13] or memristors [14–19].

Despite dramatic advancement, state-of-the-art synaptic devices with pure electronic components [4, 7–12, 20–22] are faced with a number of limitations. First, in conventional artificial synapses, neuromorphic computing is isolated from the data acquisition sensors (ocular, olfactory or auditory stimuli) [23, 24]. The lack of a neuromorphic sensing component results in undesirable hardware redundancy and system latency. Furthermore, real neuronal system always involves multiple steps of plasticity mechanism that convey considerable flexibility in the modulation of the connectivity strength [5, 25, 26]. However, the coupling coefficient of conventional artificial synapses is typically fixed, which is inadequate to emulate the complex activities of real organisms. These limitations are calling for new architectural designs and functional elements for upgrading the computing capabilities of existing neuromorphic systems. Using light-waves or photons to implement neural networks represents a potentially disruptive avenue, which offers ultrafast processing speeds, robustness,

and superior connectivity between discrete computing modules [27]. The key challenge is to fabricate an optical device that can respond to light stimulus in a neuron-like fashion (e.g. exhibiting behaviors emulating short-, long-term plasticity, and spatiotemporal processing), and in the meantime offers sufficient coupling mechanisms to either optical feedbacks or to other optical computing circuitry. While translating the neuromorphic modalities from electrical to optical domain is relatively straightforward, e.g. by driving a laser in its linear operation regime, the reverse process is non-trivial to attain in a single device.

Here we demonstrate a proof-of-concept optical neuromorphic device based on a heterostructure combining graphene and atomically thin single-walled carbon nanotubes (SWNTs) [28, 29]. In our phototransistor device, short-term plasticity (STP) behaviors are achieved through charge transfer between graphene and SWNTs in the heterostructure [29, 30], which is absent for the optically-gated pure carbon nanotube programmable devices [31]. The plasticity can be flexibly modulated by the gate voltage, which results in a dynamic synapse with *in situ* adjustable weight. In addition, due to the charge-trap rich interface between the hybrid film and the substrate, the synapse can also act as an optoelectronic non-volatile memory that features gate-controlled retention time, well emulating the long-term plasticity (LTP) through charge-trap-mediated optical coupling. Furthermore, by exciting the device with multiple light beams, we demonstrate the capability of advanced optical spike processing, i.e. optical logic operation, pointing to the potential of more sophisticated computing. The multifunctional device bridges the gap between the neuromorphic computing elements and the sensory data in real world and also represents a fundamental building block in the toolbox for emerging photonics-enabled neuromorphic networks.

2. Experimental results and discussion

The schematic of the proof-of-concept light-stimulated synapse is illustrated in figure 1(a) (see Methods for fabrication details). A defect-free single-layer graphene was identified by Raman spectroscopy (see detailed analysis in the supporting information, section S1 (stacks.iop.org/TDM/4/035022/mmedia)). The graphene-nanotube heterostructure film is used due to its strong light absorption, inherent robustness and the various methods available to tune its fundamental interfacial properties [32, 33]. In our synaptic phototransistor, the light pulse can be regarded as the pre-synaptic spikes or external stimuli, and the channel conductance is treated as the synaptic weight. The tunable transport properties of the channel, under a gate bias, provides foundation for dynamically tunable synaptic plasticity [34].

We first characterize the STP in response to optical stimulus. When a pre-synaptic light spike (405 nm, 50 μW, 5 ms) is applied, an inhibitory post-synaptic current (IPSC) is triggered, at $V_G = 0$ V. It reaches a peak value immediately after the excitation spike, and gradually recovers to its initial value (top inset of figure 1(b)). This dynamical behavior well reproduces an IPSC process observed in biological inhibitory synapse [35], a representative feature of STP. When setting the gate bias to $V_G = 20$ V, the same input light spike triggers an excitatory post-synaptic current (EPSC), which matches the behavior of an excitatory synapse [24] in organisms (the bottom inset of figure 1(b)). The recovering channel conductance can be well fitted with a double exponential function. The two relaxation times ($\tau_1 = 38$ ms and $\tau_2 = 528$ ms) are believed to be associated with the intra-layer and the inter-layer photocarrier recombination processes, respectively (see the supporting information, section S2). These synaptic responses are highly reproducible as shown in figure S2. As the ΔPSC (difference between the initial and the peak value of post-synaptic current) is an indication of the synaptic plasticity, these results prove that the plasticity of the artificial synapse can be modulated by the gate electric field. To further demonstrate *in situ* adjustment of the synaptic weight, ΔPSCs under different gate biases from -50 V to $+50$ V are studied, as plotted in figure 1(b). It should be noted that the saturation of ΔPSCs is attributed to the fact that the Fermi level of graphene is not as amendable by light excitation at relatively high gate voltage.

In neuroscience, the synaptic modification relies on the spike time or spike rate between stimuli. The spike duration-dependent inhibitory or EPSC variations of our device are shown in figure 1(c). The amplitude of ΔIPSC or ΔEPSC peak values increase with the spike duration from 5 to 100 ms. The saturated increase of the ΔPSC is attributable to the optical absorption saturation [36]. It should be mentioned that the characteristic spike duration (on the order of tens of milliseconds) that leads to effective stimulation in our device is very similar to those found in biological neurons [21, 37]. The inset of figure 1(c) shows a real optical microscope image of the synaptic transistor. The gate adjustable plasticity can be further understood by considering the energy band alignment between graphene and carbon nanotubes (figure 1(d)) which was also discussed in detail in a previous literature [30] (see also section S3 in the supporting information).

We now move to discuss the dynamic synaptic behaviors of our device. Paired-pulse facilitation (PPF) refers to a synaptic process where enhancement of transmitter release is activated by two closely spaced stimuli. PPF is considered instrumental for temporal information encoding in auditory or visual signals. Figure 2(a) schematically illustrates the effect of PPF in a biological synapse. In our device, this important temporal learning function is also mimicked. When a pair of light spikes (50 μW, 5 ms) with a time delay of 55 ms are applied to an inhibitory synapse ($V_G = 0$ V),

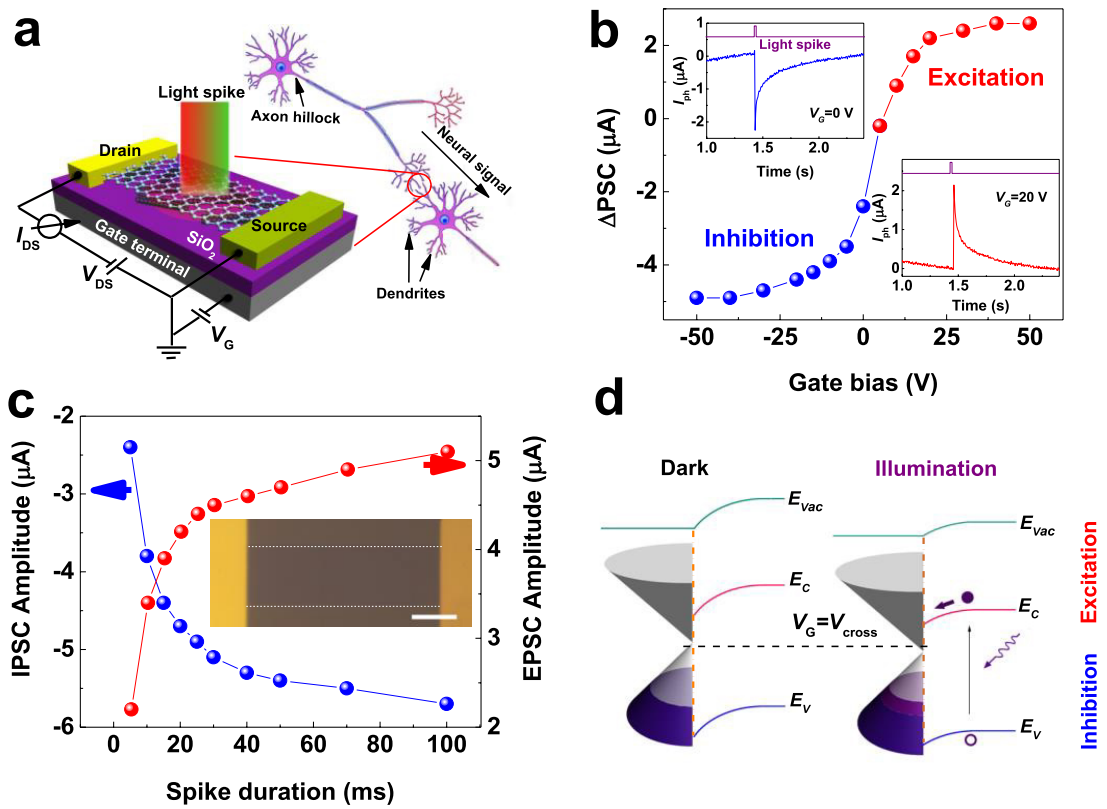

Figure 1. Light-stimulated synapse with *in situ* adjustment function. (a) Schematic illustrations of the synapse and the neural signal transmission of a biological synaptic integration in a neuron. In a biological synapse, action potentials caused by firing permits neurotransmitter release, then the signals are transmitted as a synaptic potential from the pre-synapse to the post-synapse. In the case of our artificial synapse, application of the light pulse generates several photocarriers, which contribute to the current change in the channel. (b) The change of amplitudes of PSC triggered by a pre-synaptic light spike (50 μW, 5 ms) at gate biases between −50 V and +50 V. Top inset: A typical IPSC change triggered by the light spike under $V_G = 0$ V. Bottom inset: a typical EPSC change in response to the light spike under $V_G = 20$ V. (c) Spike duration-dependent change of IPSC and EPSC for an inhibitory synapse (blue balls line, $V_G = 0$ V) and an excitatory synapse (red balls line, $V_G = 20$ V), the power of the light spike is 50 μW. The inset is the optical micrograph of the fabricated device (scale bar, 20 μm). (d) Energy-band diagram of the graphene/SWNTs interface. The built-in field formed at the interface is tuned by electrons transferred from the SWNTs layers in illumination. Purple dot, circle and arrow indicate electron, hole and photon, respectively.

the peak value of the IPSC triggered by the second pre-synaptic spike is seen appreciably larger than that by the first pre-synaptic spike, as shown in figure 2(b). The PPF index (A2/A1 × 100%), defined as the ratio of the amplitude of the second IPSC (A2) divided by that of the first IPSC (A1), is plotted as a function of Δt_{pre} (the time delay between the two consecutive pre-synaptic spikes) in figure 2(c). The PPF index reaches the maximum value (155%) when $\Delta t_{pre} = 6$ ms, and gradually decreases with increasing Δt_{pre}. This verifies that high-repetition training pulses can effectively enhance learning effect in our device, similar to the scenario in a real biologic system. The working mechanism relates to the recombination of photocarriers. When the first light spike ends, photo-generated electron–hole pairs begin to recombine. If the second spike is applied before the full recombination, the photo-excited electrons from the first spike still partially reside in the graphene channel. Consequently, photo-generated electrons triggered by the second light pulse are augmented, inducing the PPF. Similarly, the PPF function can also be obtained in an excitatory synapse ($V_G = 20$ V, see supporting information figure S4). Based on this mechanism, we have also achieved a frequency dependent synaptic transmission, which underlies many neural computations such as sound-source localization, orientation detection, by using a stimulus train consists of 10 light spikes with different frequency. The IPSC gain (A10/A1) is plotted as a function of the stimuli frequency in inset of figure 2(c). The increasing of IPSC amplitudes indicates a high-pass filtering function, enable the gain control of such artificial synaptic filter through the stimulus frequency.

Repetitive spike activity can induce a decrease or increase of synaptic efficacy in various parts of the nervous system, known as the synaptic depression or potentiation [37]. To characterize variations of the synaptic weight (herein defined by ΔPSC/initial PSC), the trends of PSC with a series of consecutive pulses (50 μW, 5 ms pulses with 10 ms intervals) at $V_G = 0$ and 20 V are measured and shown in figure 2(d). For $V_G = 0$ V, the synaptic depression characteristics (weakening of the synaptic weight) is observed. When the light pulses are applied at $V_G = 20$ V, the synaptic potentiation characteristics (strengthening of the synaptic weight) is

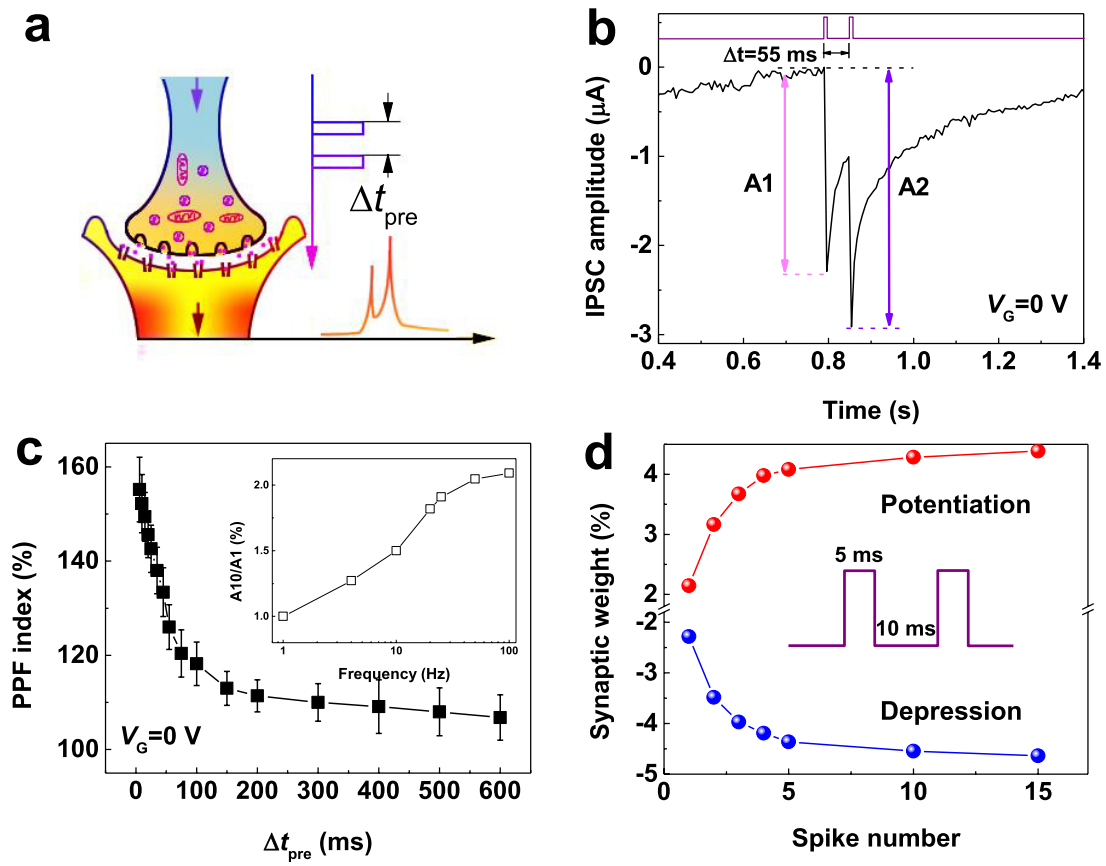

Figure 2. PPF behaviors by temporally correlated light spikes. (a) Schematics of the post-synaptic current triggered by a pair of temporally correlated pre-synaptic spikes. (b) The change of amplitude of IPSC by a pair of pre-synaptic light spikes with an inter-spike interval time of 55 ms at $V_G = 0$ V. A1 and A2 represent the amplitudes of the first and second IPSCs, respectively. (c) PPF index (A2/A1) plotted as a function of light spike interval time Δt_{pre}, which is extracted from 10 independent tests. The dots and error bars represented the average values and standard deviations, respectively. Inset: frequency-dependent IPSC gain (A10/A1) as a function of light spike frequency. (d) The depression and potentiation modulation for the inhibitory (blue balls line, $V_G = 0$ V) and excitatory (red balls line, $V_G = 20$ V) synapses operated by a series of consecutive light spikes (50 μW, 5 ms pulses with 10 ms intervals).

obtained. For both cases, the PSC rapidly changes in the first light spikes and then saturates. These results suggest that, in addition to gate-tunable behavior, our synaptic devices are also programmable through controlling the number of excitation pulses. Spike-timing-dependent plasticity (STDP) is widely accepted as a synaptic learning rule in bioscience, where the synaptic modification relies on relative timing of neuronal activity [38]. And different forms of STDP that reflect the diversified information processing and storage needs have been measured due to different superposition and coincidence of the specific physiological mechanisms [39]. Simplified symmetric STDP is implemented in our synaptic transistor, which is related to hippocampus-like associative learning and more details is described in section S5 of supporting information.

Multiple categories of synaptic plasticity allow synapses to perform wildly different functions in information processing [6]. Note that in real biological systems, distinct biochemical mechanisms are typically responsible for STP and LTP, respectively. In our device, thanks to the geometry of the graphene-SWNT nanostructure, effects from substrate surface traps can be harnessed to emulate LTP through charge-trap-mediated optical coupling.

In figure 3(a) we show the variation of synaptic weight triggered by a long-duration pre-synaptic light spike (50 μW, 100 ms) under a negative gate bias. An accessional resistance is directly triggered but does not relax back to its initial state at $V_G = -20$ V, signifying a LTP formation. Experimentally, this LTP effect may be mitigated by reducing the amplitude of negative gate voltage, i.e. applying a -10 V or zero bias. The underlying physical mechanism again originates from photo-gating effect. Specifically, photo-generated carriers are captured by trap centers (such as dangling bonds, intrinsic defects and local structural distortions) [40] at the substrate surface. Figure 3(b) schematically illustrates this charge trapping process. Under a negative gate electric field, photo-generated holes in graphene or SWNTs are partially trapped into the trap sites, which results in a long-term stable photo-gating effect even after the incident light is switched off due to the high trapping energy barrier. The LTP signal level is determined by the trap density. Tuning the number of the traps by gate electric field effectively adjusts the LTP levels (figure 3(a)). Electrical field controlled charging/discharging of traps as well as the hysteresis loop direction of the transfer characteristics verify that the trap centers are of Coulomb type (see supporting

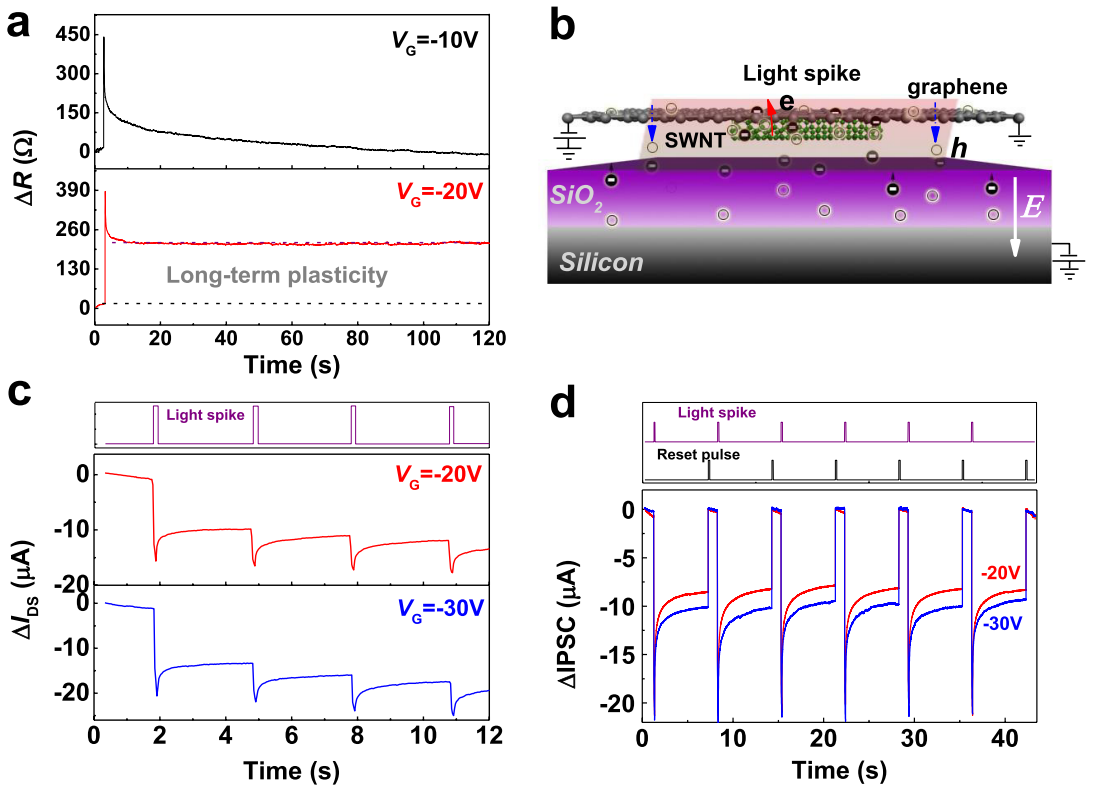

Figure 3. Gate-dependent LTP formation in the artificial synapse. (a) The amplitude of IPSC triggered by a long-duration pre-synaptic light spike (50 μW, 100 ms) at $V_G = -10$ V and -20 V, respectively. (b) Schematic illustration of LTP formation mechanism, photo-generated holes from the graphene FET channel or SWNTs are captured at the surface of silicon dioxide due to the existence of the defects. The white arrow indicates the direction of the electric field for negative gate voltages. (c) The amplitude of IPSCs triggered by a serial of consecutive spikes (100 ms pulses spaced 3 s apart with 50 μW average power) at different gate bias, showing enhancement of LTP effect. (d) Gate voltage-dependent amplitudes of IPSC and reset switching operations by the gate bias pulses.

information figure S5). To further examine the role of light pulse played in the LTP process, we measured the response at different illumination power (see supporting information figure S6). With increasing incident light power, it is found that photo-induced carrier concentration rapidly increases. As a result, more carriers are trapped, leading to enhanced hysteresis window in the transfer characteristics. The effective trapping charges density can be calculated based on the electron transport characteristic [19, 40], and the trapped charge density is about $n = 5.1 \times 10^{11}$ cm^{-2} under the light illumination of 200 μW (see section S6, suppoting information for detailed analysis). These phenomens consistently support the view that photo-excitation and gate voltage are both responsible for the memory effect observed. The variability of trap density between devices is especially critical for the future integrated neural architecture performance [41]. So we have summarized statistics distribution of trap density in 25 synaptic devices under 200 μW illumination, and the coefficient of variance (the ratio of standard deviation to mean value) is only about 4.8%, which may be sufficient for the neural circuits with capable of tolerance.

Figure 3(c) displays the synaptic response upon consecutive spike irradiation, under a gate voltage of -20 V and -30 V, respectively. Clearly, enhancement of long-term memory, as observed in biological system [26], is emulated. In real biological systems, long-term potentiation can be activated by the pre-synaptic action potentials, such as high-frequency stimulation [19]. In our device, the higher stimulus frequency leads to a larger change in IPSC in the same effective time, indicating that more carries are trapped with high frequency excitation (see supporting information figure S8). In figure 3(d), nulling of the plasticity current by a positive 'reset' gate pulse is observed. This reversed electric pulse could redistribute the trap centers and facilitate de-trapping process. These results demonstrate that our synapses can go beyond simply mimicking synaptic biological characteristics, and may also be designed as rewriteable non-volatile optical memory cells [42] or optoelectronic switches, thereby enabling more device functionalities.

We then show the use of our photosensitive devices for emulating a conceptual axon-multi-synapses network [43]. Figure 4(a) schematically illustrates the structure of the biological and artificial synaptic networks. In our setup, drawing on wavelength-division-multiplexing (WDM) and broadband light absorption in the all-carbon hybrid film [29], we use different wavelengths to represent distinct pre-synaptic channels. Essentially, we find that our device obeys two summation rules, namely super-linear temporal

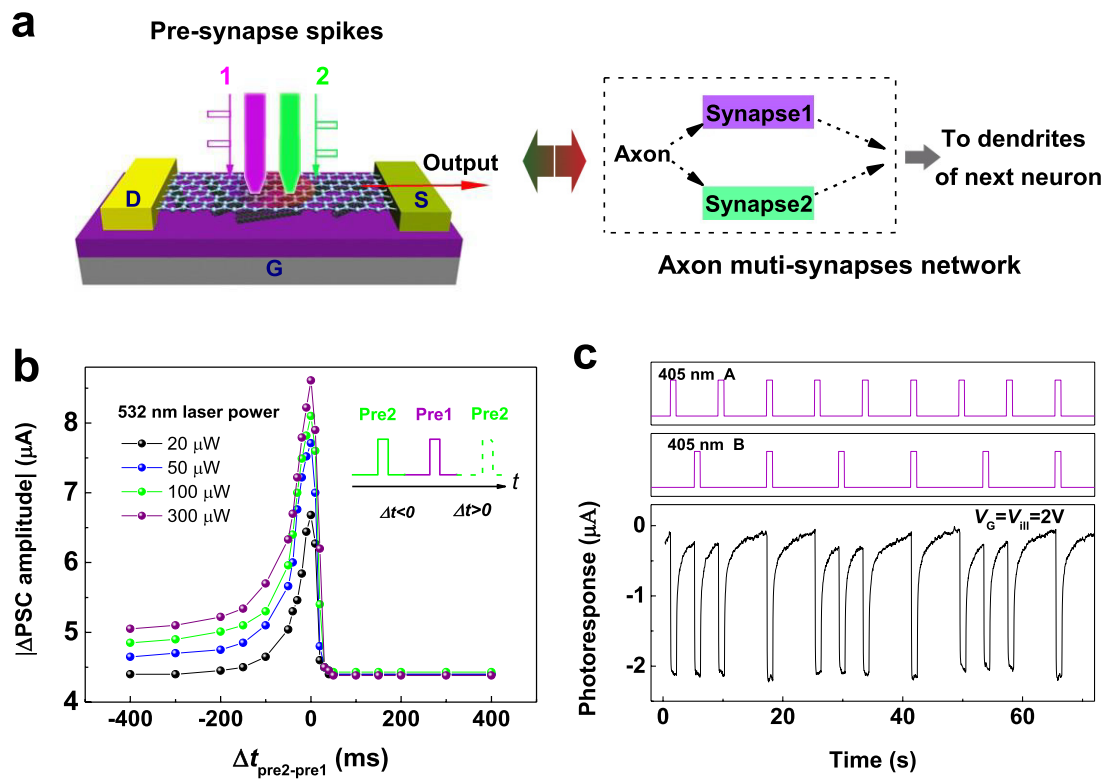

Figure 4. WDM network and optical logic operations. (a) Schematic illustrations of the multi-neural signals transmission in a biological system and a compact artificial axon-multi-synapses network employing multiple light stimuli. (b) The change of PSC amplitude at the trailing edge of pre-synapse1 spike as a function of $\Delta t_{\text{pre2-pre1}}$ between the two presynaptic spikes (duration 20 ms with different power for 532 nm and fixed power 405 nm spikes) at $V_G = 0$ V. (c) The time response of an NOR logic operation by utilizing two 405 nm light spikes (10 μW, 1 s) as logic input signals at V_{ill} (~2 V in this irradiation operation).

summation rule and sub-linear power summation rule [43, 44]. On one hand, we test the photoresponse of the device stimulated by two laser pulses (405 nm and 532 nm light pulses, defined as pre-synapse1 and pre-synapse2) at $V_G = 0$ V. The sum IPSC current, measured at the trailing edge of pre-synapse1 spike, as a function of the delay $\Delta t_{\text{pre2-pre1}}$ is plotted in figure 4(b). When $\Delta t_{\text{pre2-pre1}} = 0$, the two pre-synaptic spikes are applied simultaneously where a pronounced total ΔPSC appears in the post-synaptic neuron. With increasing $|\Delta t_{\text{pre2-pre1}}|$, the spatiotemporal amplitude summation decreases asymmetrically, as typically expected [8]. Spatiotemporally correlated photoresponse under multiple laser spikes is thus achieved, where the total amplitude response is also dependent on photonic intensity (inset of figure 4(b)) that is great valuable for the thresholding in future neuromorphic circuits. On the other hand, we also study the statistics of the synaptic output when two spikes with different power levels are simultaneously applied to the device (see supporting information figure S9). Briefly, we compare the measured and theoretical arithmetic sum of the two separated IPSCs. It is found that close-to-linear spatial summation applies in the low power regime (where IPSC does not saturate), although this transits to a sublinear-dependence by increasing either spikes' power into the saturation regime. It is worth mentioning that the observed sub-linear summation rule is analogous to the action of a soma cell [39].

The rich physics associated with hot-carriers in graphene and charge transfer dynamics at the graphene-SWNTs interface make our device a unique platform for achieving complex computing capabilities. To demonstrate optical processing on light spikes, we employ one of the light channels (405 nm spike B) to conceptually denote a neuromorphic feedback signal and demonstrate optical NOR, AND and OR logic operations on the stimuli (405 nm spike A). It is worth pointing out that we choose to demonstrate logic operations due to its generic nature. In principle, the function generation can be readily extended to neuromorphic tasks. Specifically, setting the gate bias close to V_{ill} (a crossover gate of the transfer curves under spike A or B channel individual illumination and under both A and B channels simultaneously illumination), NOR basis logic operations could be demonstrated: a negative output current is triggered when either individual pre-synapse stimulation or both pre-synapses stimulation are applied simultaneously, as plotted in figure 4(c). Furthermore, AND logic operation is performed based on the super-linear temporal summation rule. When the gate bias is set close to V_{cross}, a very low output current is obtained under individual pre-synapse stimulation. However, if both pre-synapses trigger simultaneously, super-linear summation rule would apply and guarantee a significant output (see supporting information figure S10(a)). On the other hand, sub-linear power summation rule dictates in the OR operation: setting

the gate bias at $V_G = 20$ V, the device is operating in the EPSC saturation regime, where any pre-synaptic pulse would trigger a high output current. Sub-linear power summation rule ensures that the output current does not change much even both pulses are applied (see supporting information figure S10(b)).

It should be noted that it is important for a photonic synaptic device to have effective coupling with external light fields as it may open up a number of possibilities to enable flexibly configured computing architecture. The coupling mechanism could help integrate a feedback signal from a photonics based neural network, or it may simply act as an interface to a dedicated non-neuromorphic optical computing resources. By engineering our phototransistor channel to allow for evanescent light coupling with underlying waveguide, it is feasible to realize fully integrated photonic neuromorphic systems [45, 46].

3. Conclusion

In summary, we have demonstrated a novel-concept light-activated synaptic device based on a graphene-carbon nanotube heterostructure phototransistor. Both short-term and long-term synaptic plasticity are successfully mimicked in our device. The unprecedented flexibility in plasticity tuning via a gate field ensures programmable networking capabilities. Our device not only acts as an optical computing node that is functionally equivalent to today's electrically-driven artificial synapse, but also may render simpler neuromorphic vision signal processing. Furthermore, advanced optical spike processing (NOR and AND/OR logic operations) are demonstrated, providing an important foundation for more sophisticated computing. With silicon-compatible fabrication, full set of synaptic functionalities, as well as potential advantages in terms of processing speeds and parallelism, such an optically-driven artificial synapse represents an important step forward in realizing the next generation photonics-enabled neuromorphic sensing and computing.

4. Methods

4.1. Fabrication of artificial synapse based on phototransistor

The graphene samples were grown on copper foil by CVD method, and Raman spectroscopy combined with optical microscope characterizations point to a defect-free single-layer sample. The single-wall carbon nanotubes (SWNTs) were purchased from a commercial supplier (Carbon solutions Inc.). To fabricate a proof-of-concept artificial synapse, SWNT suspensions are produced by ultrasonicating 2 mg nanotube in 20 ml NMP, and then the resulting suspensions ultra-centrifuged with 10 000 g for 1 h was coated onto a Si/SiO_2 (285 nm) wafer. CVD graphene is transferred on top of the SWNT layer using the poly(methyl methacrylate) supported procedures. Subsequently, different metal composition (Ti/Au and Pd/Au) as the source and drain electrodes are patterned by standard photolithography. Graphene channel fabrication is patterned by another photolithography and oxygen plasma etching. For simulating synaptic functions, we employ 405 and 532 nm laser diodes as pre-synapse spikes, respectively. The beam is guided through an optical fiber with a FC/PC ferrule and is subsequently incident onto the channel of the devices without focusing. The beam at the device was measured to be Gaussian-shaped with a diameter of about 300 μm (at 405 nm illumination). The area of the channel is about 90 μm $\times$ 30 μm.

4.2. Electrical measurements

Electrical performance of the transistors and synaptic simulation measurements are carried out by a semiconductor parameter characterization system (Keithley 4200 SCS) in a closed probe station under vacuum (10^{-6} Torr) at room temperature. Pre-synaptic light spikes are applied on the graphene channel, and post-synaptic current is measured by applying a source-drain voltage of 0.5 V. To verify the universality of the operation of our optical synapses, excitatory/inhibitory post-synaptic currents and PPF stimulated by spikes from five synaptic devices are measured.

4.3. Raman spectrum

Raman measurements were performed in a Horiba Jobin Yvon LabRAM HR 800 system using a 514 nm excitation laser operating at 1 mW, $\times$100 objective lens with about 1 μm diameter spot size, and 1800 lines mm^{-1} grating with about 0.45 cm^{-1} spectral resolution.

Acknowledgments

This work was supported in part by National Basic Research Program of China (2017YFA0206304, 2013CB932900, 2014CB921101, 2011CB301900); National Natural Science Foundation of China (61378025, 61427812, 61274102, 61504056); National Youth 1000-Talent Plan; A 'Jiangsu Shuangchuang Team' Program.

Additional information

Supporting information is available.

Competing financial interests

FW, SCQ, YJL, YX, and RZ have filed a Chinese patent based on this work (application no. 201610848037.9).

Author contributions

FQW, XMW conceived the project and together with YS and RZ supervised the project. QW, XRW,

YS designed the optical neuromorphic experiment, SCQ, YJL prepared the devices and performed all the optical characterizations. YBX contributed to the interpretation of plasticity mechanisms. FQW, XMW co-wrote the paper with all authors contributing to discussion and preparation of the manuscript.

ORCID iDs

Fengqiu Wang https://orcid.org/0000-0001-9823-5788

References

[1] Merolla P A *et al* 2014 A million spiking-neuron integrated circuit with a scalable communication network and interface *Science* **345** 668–73
[2] Koelmans W W *et al* 2015 Projected phase-change memory devices *Nat. Commun.* **6** 8181
[3] Shepherd G M 2004 *The Synaptic Organization of the Brain* (New York: Oxford University Press)
[4] Prezioso M *et al* 2015 Training and operation of an integrated neuromorphic network based on metal-oxide memristors *Nature* **521** 61–4
[5] Destexhe A and Marder E 2004 Plasticity in single neuron and circuit computations *Nature* **431** 789–95
[6] Abbott L F and Regehr W G 2004 Synaptic computation *Nature* **431** 796–803
[7] Jo S H *et al* 2010 Nanoscale memristor device as synapse in neuromorphic systems *Nano Lett.* **10** 1297–301
[8] Kim K, Chen C L, Truong Q, Shen A M and Chen Y 2013 A carbon nanotube synapse with dynamic logic and learning *Adv. Mater.* **25** 1693–8
[9] Chang T, Jo S H and Lu W 2011 Short-term memory to long-term memory transition in a nanoscale memristor *ACS Nano* **5** 7669–76
[10] Yu S *et al* 2013 A low energy oxide-based electronic synaptic device for neuromorphic visual systems with tolerance to device variation *Adv. Mater.* **25** 1774–9
[11] Shi J, Ha S D, Zhou Y, Schoofs F and Ramanathan S 2013 A correlated nickelate synaptic transistor *Nat. Commun.* **4** 2676
[12] Pickett M D, Medeiros-Ribeiro G and Williams R S 2013 A scalable neuristor built with Mott memristors *Nat. Mater.* **12** 114–7
[13] van de Burgt Y *et al* 2017 A non-volatile organic electrochemical device as a low-voltage artificial synapse for neuromorphic computing *Nat. Mater.* **16** 414–8
[14] Shen A M *et al* 2013 Analog neuromorphic module based on carbon nanotube synapses *ACS Nano* **7** 6117–22
[15] Sangwan V K *et al* 2015 Gate-tunable memristive phenomena mediated by grain boundaries in single-layer MoS_2 *Nat. Nanotechnol.* **10** 403–6
[16] Strukov D B, Snider G S, Stewart D R and Williams R S 2008 The missing memristor found *Nature* **453** 80–3
[17] Bessonov A A *et al* 2015 Layered memristive and memcapacitive switches for printable electronics *Nat. Mater.* **14** 199–204
[18] Mandal S, El-Amin A, Alexander K, Rajendran B and Jha R 2014 Novel synaptic memory device for neuromorphic computing *Sci. Rep.* **4** 5333
[19] Mandal S, Long B and Jha R 2013 Study of synaptic behavior in doped transition metal oxide-based reconfigurable devices *IEEE Trans. Electron Devices* **60** 4219–25
[20] Ohno T *et al* 2011 Short-term plasticity and long-term potentiation mimicked in single inorganic synapses *Nat. Mater.* **10** 591–5
[21] Kuzum D, Yu S and Wong H S 2013 Synaptic electronics: materials, devices and applications *Nanotechnology* **24** 382001
[22] Tian H *et al* 2016 Anisotropic black phosphorus synaptic device for neuromorphic applications *Adv. Mater.* **28** 4991–7
[23] Cassenaer S and Laurent G 2012 Conditional modulation of spike-timing-dependent plasticity for olfactory learning *Nature* **482** 47–52
[24] Lee W C *et al* 2016 Anatomy and function of an excitatory network in the visual cortex *Nature* **532** 370–4
[25] Hare T A, Camerer C F and Rangel A 2009 Self-control in decision-making involves modulation of the vmPFC valuation system *Science* **324** 646–8
[26] Harvey C D and Svoboda K 2007 Locally dynamic synaptic learning rules in pyramidal neuron dendrites *Nature* **450** 1195–200
[27] Rosenbluth D, Kravtsov K, Fok M P and Prucnal P R 2016 A high performance photonic pulse processing device *Opt. Express* **17** 22767–72
[28] Yan Z *et al* 2014 Rebar graphene *ACS Nano* **8** 5061–8
[29] Liu Y *et al* 2015 Planar carbon nanotube-graphene hybrid films for high-performance broadband photodetectors *Nat. Commun.* **6** 8589
[30] Liu Y *et al* 2016 Charge transfer at carbon nanotube-graphene van der Waals heterojunctions *Nanoscale* **8** 12883–6
[31] Agnus G *et al* 2010 Two-terminal carbon nanotube programmable devices for adaptive architectures *Adv. Mater.* **22** 702–6
[32] Lv R, Cruz-Silva E and Terrones M 2014 Building complex hybrid carbon architectures by covalent interconnections: graphene-nanotube hybrids and more *ACS Nano* **8** 4061–9
[33] Zhu Y *et al* 2012 A seamless three-dimensional carbon nanotube graphene hybrid material *Nat. Commun.* **3** 1225
[34] Tian H *et al* 2015 Graphene dynamic synapse with modulatable plasticity *Nano Lett.* **15** 8013–9
[35] Chih B, Engelman H and Scheiffele P 2005 Control of excitatory and inhibitory synapse formation by neuroligins *Science* **307** 1324–8
[36] Mueller T, Xia F and Avouris P 2010 Graphene photodetectors for high-speed optical communications *Nat. Photon.* **4** 297–301
[37] Bi G Q and Poo M M 1998 Synaptic modifications in cultured hippocampal neurons: dependence on spike timing, synaptic strength, and postsynaptic cell type *J. Neurosci.* **18** 10464–72
[38] D'Amour J A and Froemke R C 2015 Inhibitory and excitatory spike-timing-dependent plasticity in the auditory cortex *Neuron* **86** 514–28
[39] Ho V M, Lee J A and Martin K C 2011 The cell biology of synaptic plasticity *Science* **334** 623–8
[40] Wang H, Wu Y, Cong C, Shang J and Yu T 2010 Hysteresis of electronic transport in graphene transisstors *ACS Nano* **4** 7221–8
[41] Mandal S, Long B, El-Amin A and Jha R 2013 Doped HfO_2 based nanoelectronic memristive devices for self-learning neural circuits and architecture *IEEE/ACM Int. Symp. on Nanoscale Architectures (NANOARCH)*, (*Brooklyn, NY*) pp 13–8
[42] Roy K *et al* 2013 Graphene-MoS_2 hybrid structures for multifunctional photoresponsive memory devices *Nat. Nanotechnol.* **8** 826–30
[43] Toni N, Buchs P A, Nikonenko I, Bron C R and Muller D 1999 LTP promotes formation of multiple spine synapses between a single axon terminal and a dendrite *Nature* **402** 421–5
[44] Polsky A, Mel B W and Schiller J 2004 Computational subunits in thin dendrites of pyramidal cells *Nat. Neurosci.* **7** 621–7
[45] Shen Y *et al* 2017 Deep learning with coherent nanophotonic circuits *Nat. Photon.* **11** 441–6
[46] Woods D and Naughton T J 2012 Photonic neural networks *Nat. Phys.* **8** 257–9